Available online at www.sciencedirect.com

ScienceDirect

Ceramics International 40 (2014) 2965–2971

CERAMICS INTERNATIONAL

www.elsevier.com/locate/ceramint

Synthesis and characteristics of fly ash and bottom ash based geopolymers–A comparative study

Ehsan ul Haq*, Sanosh Kunjalukkal Padmanabhan, Antonio Licciulli

Department of Engineering for Innovation, University of Salento, Lecce 73100, Italy

Received 23 September 2013; received in revised form 1 October 2013; accepted 1 October 2013
Available online 11 October 2013

Abstract

The research was carried out to develop geopolymers mortars and concrete from fly ash and bottom ash and compare the characteristics deriving from either of these products. The mortars were produced by mixing the ashes with sodium silicate and sodium hydroxide as activator solution. After curing and drying, the bulk density, apparent density and porosity, of geopolymer samples were evaluated. The microstructure, phase composition and thermal behavior of geopolymer samples were characterized by scanning electron microscopy, XRD and TGA-DTA analysis respectively. FTIR analysis revealed higher degree of reaction in bottom ash based geopolymer. Mechanical characterization shows, geopolymer processed from fly ash having a compressive strength 61.4 MPa and Young's modulus of 2.9 GPa, whereas bottom ash geopolymer shows a compressive strength up to 55.2 MPa and Young's modulus of 2.8 GPa. The mechanical characterization depicts that bottom ash geopolymers are almost equally viable as fly ash geopolymer. Thermal conductivity analysis reveals that fly ash geopolymer shows lower thermal conductivity of 0.58 W/mK compared to bottom ash geopolymer 0.85 W/mK.

Keywords: C. Thermal conductivity; Geopolymer; Bottom ash; Fly ash; Mechanical strength

1. Introduction

Coal is the largest source of energy for the generation of electricity worldwide accounting for approximately 36% of the world′s electricity production. This situation is likely to remain until at least 2020. A huge amount of fly ash and bottom ash is produced during coal burning posing an increasing concern in its recycling. The ashes are either dumped for the landfill purposes or used in construction. One of the emerging applications of ashes in construction nowadays is the manufacture of so called geopolymers binders as an alternative to Portland cement. Geopolymer is an alkali-activated aluminosilicates which is able to produce a Si–O–Al framework, reacting at low temperatures. The name was given by Joseph Davidovits in 1970s [1]. There are four steps in a geopolymerization reaction: (i) dissolution of Al and Si oxides from the ash aluminosilicate due to the strong alkaline liquid attack, (ii) formation of oligomers by polymerization like Si–O–Si and Si–O–Al bonds, (iii) formation of three dimensional aluminosilicate structures by polycondensation of the oligomers and (iv) bonding of the remaining solid filler particles to the aluminosilicate network for further enhancing the strength and stability [2,3]. The whole process is helped by molecular thermal agitation which can be successfully provided by heating at 60–80 °C in the humid atmosphere for 24–48 h to complete the reaction, although the strength continues to increase as the time passes and the reaction goes to completion [4]. There are evidences showing that same process can be accomplished by microwave radiations for few minutes of curing [5–6]. Temuujin et al. have reported preparing the geopolymer at ambient temperature by slightly changing the composition by introducing slag or high calcium source [7]. In the entire process water mobilizes the ions and reactants, and facilitates the mold ability of mortar, and evaporates during curing and drying process [8]. The precursors of geopolymers are usually aluminosilicate source (fly ash, clay), sodium silicate in aqueous solution (water glass), sodium hydroxide and water. The concentration of sodium silicate is found to be the best around 14 M in water [9–10]. Fly ash is not only a by-product that is produced in abundance

*Corresponding author. Tel.: +39 32 7996 6738; fax: +39 83 2183 0130.
E-mail addresses: amonehsan@hotmail.com, amonehsan@gmail.com (E. ul Haq).

0272-8842/$ - see front matter © 2013 Elsevier Ltd and Techna Group S.r.l. All rights reserved.
http://dx.doi.org/10.1016/j.ceramint.2013.10.012

but also creates better and high strength geopolymer as compared to bottom ash. Although bottom ash and fly ash have similar chemical compositions, bottom ash is found to be less reactive compared to fly ash thus having little or almost no use in the manufacturing of geopolymer [11]. The present research is made to investigate and compare geopolymer properties from bottom ash as well as from fly ash precursors. Bottom ash is produced 10–20% during coal combustion in power plants, and 80–90% product is fly ash. Temuujin et al. and Sarker et al. have reported the best composition with optimal properties of geopolymer mortar being 73% fly ash, 18% water glass, 7% 14 M sodium hydroxide solution and 2% water [9,10]. In the present work, we used Sarker composition to make fly ash and bottom ash geopolymer mortars and investigated the changes in physical and chemical properties of the materials being produced.

2. Materials and method

2.1. Materials

Bottom ash (BA) and fly ashes (FA) were provided by ENEL (coal fired power plant Federico II, Brindisi, Italy). The other raw materials used for the experiments were water glass (sodium silicate solution with 9% Na_2O, 30% SiO_2 and 61% H_2O with specific gravity of 1.35 g/cm^3) and 14 M sodium hydroxide solution prepared by dissolving sodium hydroxide pellets in water.

2.2. Preparation of mortar

The mortars were prepared by mixing ashes (bottom ash or fly ash), water glass, sodium hydroxide and water in a ceramic jar and milling in a planetary ball mill for 10 min using zirconia balls as grinding media to get homogenized slurry. The composition of the slurries is shown in the Table 1. Water may be added later in order to enhance the plasticity and castability of the mixture during forming or casting according to the best required amount but with much care because excess water is detrimental for the properties of geopolymer. After milling, the slurry was transferred to polyethylene cylindrical molds of dimensions 3.6 cm diameter and 6 cm height and closed using a lid to avoid the moisture loss during curing. The samples were cured for 48 h at 65 °C, demolded and cured at the same temperature for another 72 h to remove the moisture. Then the samples were dried for another 96 h at ambient temperature. The samples were named as FAG and BAG respectively for fly ash and bottom ash derived geopolymer mortars. After drying, the physical and chemical properties of the geopolymer samples were characterized.

Table 1
Composition of geopolymer used in this study.

Material	Proportion by weight (%)
Fly ash or bottom ash	73
Water glass (Na_2SiO_3)	18
14 M NaOH	7
Water	2

2.3. Samples analysis

Chemical compositions of both ashes were measured by X-ray fluorescence spectrometer (Bruker M4 Tornado). Fly ash particles specific surface area was measured using BET surface area analyzer (Quantachrome *NOVA*). Apparent densities of the ashes were measured using helium Pycnometer (Quantachrome). Particle size distributions of ashes were evaluated using particle size analyzer (Cilas 1190).

Thermogravimetric analysis (TGA) and differential thermal analysis (DTA) were simultaneously performed on the geopolymer samples from 25 °C to 1000 °C (Mettler Toledo). Fourier transformation infrared spectroscopy was performed using ATR spectrometer (Attenuated Total Reflectance; Perkin-Elmer) with diamond crystal as a probe. X-ray diffraction (XRD) analysis was performed using a (Rigaku diffractometer, with Cu Kα radiations generated at 40 kV and 20 mA). The morphology of raw ashes and geopolymer mortars were evaluated by scanning electron microscopy (Model: Zeiss, Jena, Germany) analysis. Bulk density was measured by simply measuring the weight and volume while apparent density measured by using helium Pycnometer (Quantachrome). Open porosity was calculated using apparent density and bulk density by the following relation.

$$\text{Porosity } (\%) = (1 - \rho_b/\rho_a) \times 100$$

Where, ρ_b is the bulk density and ρ_a is the apparent density. Thermal conductivity of geopolymer samples were measured using a thermal conductivity analyzer C-Therm, SETARAM, a modified transient plane source technology for thermal conductivity measurements. After curing the samples were tested for compressive strength using universal testing machine (METROCOM) applying ASTM C109 standard protocol.

3. Results and discussion

3.1. Ashes analysis

Chemical compositions of both ashes, as determined on X-ray fluorescence are presented in Table 2. The major part includes SiO_2, Al_2O_3, CaO and Fe_2O_3 in both types of ashes. Calcium oxide is found to be higher in amount in fly ashes as compared to bottom ash. Fly ash particles have specific surface area of 10.14 m^2/g whereas bottom ash has 2.43 m^2/g. Particle size distribution of both the ashes is presented in Fig. 1. The mean diameter of the particles of the fly ash is 29 μm whilst for the bottom ash is 121 μm. The bottom ash particles are coarser as compared to fly ash particles also revealed in BET surface area analysis.

3.2. XRD analysis

X-ray diffraction analysis was carried out to investigate the different phases present in the ashes and geopolymers after

Table 2
Composition of fly ash and bottom ash as determined by XRF analysis (mass (%)).

Composition (%)	Bottom ash (BA)	Fly ash(FA)
Al_2O_3	27	24.33
SiO_2	46.2	42.72
K_2O	1.41	2.24
CaO	9.07	15.14
TiO_2	2.6	3.02
Cr_2O_3	0.03	0.09
Fe_2O_3	10.61	10.64
NiO	0.01	0.03
MnO	0.11	0.01
SrO	0.41	0.7

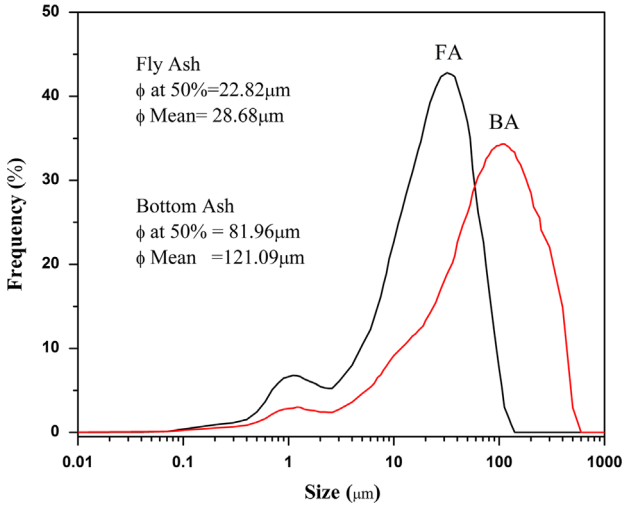

Fig. 1. Particle size distribution of fly ash and bottom ash.

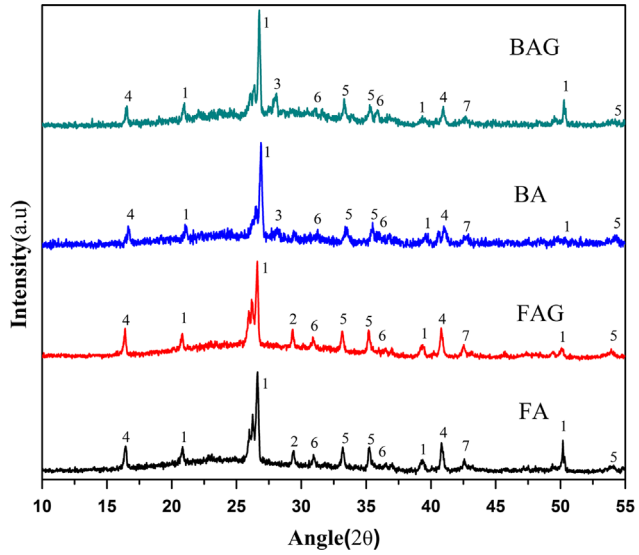

Fig. 2. XRD pattern of fly ash and bottom ash (1=Quartz, 2=Calcite, 3=Anorthite, Albite, 4=Mullite, 5=Hematite, 6=Belite, and 7=Wustite.).

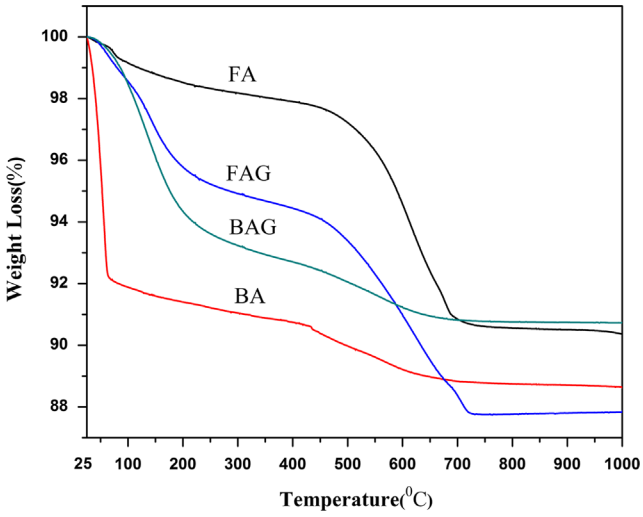

Fig. 3. Thermogravimetric analysis of ashes and geopolymer.

seven days of processing according to the schedule. The X-ray diffraction patterns of raw ashes as well as their respective geopolymers are shown in Fig. 2. For the fly ash a hump, under the quartz peak, indicates the presence of relatively more amorphous phase compared to bottom ash displaying higher amount of crystalline phases. The major crystalline phase observed in ashes as well as their geopolymers is quartz phase (JCPDS 5-0490). Along with quartz phase, other phases present in ashes as well as in their respective geopolymers are mullite (JCPDS 15-0776) and hematite (JCPDS 33-0664). Apart from these phases, XRD pattern of fly ash and its geopolymer shows peak corresponding to calcite phase (JCPDS 86-2334). Calcite in the FAG is lower than the fly ash because some of this was converted to other compound like C_3AH_6 and C_4AH_{13} as will be realised in DTA analysis. On the other side, instead of calcite peak, anorthite (JCPDS 89-1462) and albite (JCPDS 20-0554) (plagioclase feldspar member) are present in the XRD pattern of bottom ash as well as in its geopolymer [12,13]. FeO is present in the form of wustite (JCPDS 43-1312) while belite (Ca_2SiO_4) (JCPDS 9-351) peaks were also detected [14,15]. C_3AH_6 and C_4AH_{13} peaks are very low in the geopolymer XRD, indicating that minute amounts were produced during geopolymerization.

3.3. Thermogravimetric analysis

Thermogravimetric results show different trends in weight loss of fly ash and bottom ash as reported in Fig. 3. Fly ash has less water contents and this little amount of water is because of the moisture absorbed during handling and transportation. The TGA curve of fly ash shows a gradual weight loss from 100 °C to 450 °C because of absorbed moisture during handling and transportation. A major weight loss is observed from 450 °C to 750 °C, attributed to oxidation and combustion of unburnt coal entrapped inside the fly ash particles. From 750 °C onward weight loss is reduced although it continues to decrease up to 1000 °C and beyond. On the other hand TGA of BA shows quite different behavior as compared to FA because of the

inherent presence of excess of water; absorbed during cooling with water at power plant. Bottom ash loses 8% of weight just at 70 °C, which is due to evaporation of water. From 70 °C to around 430 °C, there is a gradual weight loss, which is due to evaporation of physio-chemically bonded water molecules with the bottom ash particles. Further from 430 °C to 730 °C there is another visible loss which is due to burning of the organic contents. The weight loss from 430 °C to 730 °C is around 2% while for fly ash is around 7%. This shows that fly ash contains more amount of unburnt carbon compared to bottom ash. Consequently TGA of (FAG) shows different thermal behavior compared to raw fly ash. A weight loss of 5% up to 300 °C is observed for FAG sample because of higher water content that loses up to 300 °C whereas for raw fly ash the weight loss is just 2% upto 450 °C, where almost all the water is lost. This is because the fly ash contains physically absorbed water or moisture which is lost at lower temperature whilst its geopolymer (FAG) has chemically bonded hydroxyl group to silicon (Si–OH), which is released at higher temperatures and gives Si–O–Si structure [16].

$$2Si-OH \rightarrow Si-O-Si+H_2O\uparrow$$

This reaction played a vital role in the present research because during post curing for 72 h at 65 °C, the Si–OH bonds were transformed to Si–O–T(T:Si or Al) form; increasing the connectivity, strength and stability. The weight loss behavior of (BAG) is similar to (FAG) upto 300 °C. The geopolymers continue to lose the weight till 300 °C and then the rest is similar to TGA of their respective ashes because after geopolymerization the carbon content remains the same [17].

3.4. Differential thermal analysis

The DTA behavior of ashes and their respective geopolymers are shown in Fig. 4. Differential thermal analysis was carried out simultaneously with the TGA, revealing some interesting results that not only confirm the TGA results but also evidences the presence of different compounds or phases in the ashes and geopolymers. There are many peaks indicating the presence of different transformations among different kinds of compounds present in fly ash and bottom ash. The DTA curve of bottom ash shows a big endothermic peak around 70 °C due to evaporation of water whereas fly ash does not show such a peak. The DTA of geopolymers show entirely different behavior compared to their respective ashes. The curve does not have any sharp peak instead it shows long sagging because of heat absorbance by chemically combined Si–OH form instead of free water molecule. Hence it takes higher level of heating and time to evaporate. At around 222 °C, both geopolymers show two identical but smaller peaks indicating the dehydroxylation of C_4AH_{13} ($4CaO \cdot Al_2O_3 \cdot 13H_2O$). Upon further heating similar peaks are observed at 310 °C due to the dehydroxylation of C_3AH_6 ($3CaO \cdot Al_2O_3 \cdot 6H_2O$). These cementing compounds are formed by calcium present in the ashes during geopolymerization [18–20]. From 500 to 700 °C, FA and its geopolymer (FAG) show a big exothermic hump because of the larger

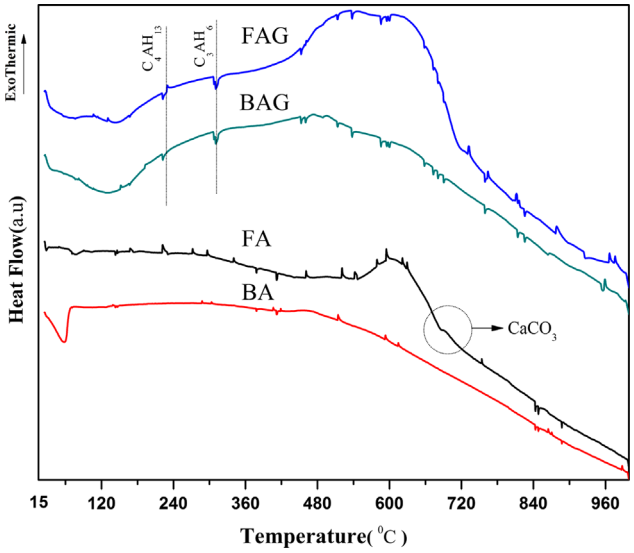

Fig. 4. Differential thermal analysis of ashes and geopolymer.

amount of unburned carbon present [17,21]. The hump for the fly ash is lower compared to its geopolymer because carbon in fly ash was encapsulated by a layer of aluminosilicate whereas in its geopolymer it is exposed due to removal of the alumina silicate layer during its activation. Later a kink in the fly ash curve is observed at around 700 °C indicating the decomposition of $CaCO_3$ (calcite), and not present in the bottom ash. This decomposition kink is absent in the FAG because some calcium has been transformed to C_4AH_{13} and C_3AH_6. The reason being, whenever the amount of sodium hydroxide activator solution is higher than 4 wt%, the decomposition peak of calcite in DTA is covered by the big exothermic hump produced by the oxidation of free carbon exposed to air due to dissolution of surface layer of the cenosphere during activation by sodium hydroxide solution [19].

3.5. Infrared spectra

FTIR was used to study the effect of geopolymerization on both types of ashes, qualitatively and quantitatively. For bottom ash, typical bands of –OH bending and stretching of absorbed water are at 1640 and 3340 cm^{-1} respectively as shown in Fig. 5. Whereas these bands are almost absent in fly ash. The presence of excess water in bottom ash as compared to fly ash has also been observed in TGA and DTA analysis. In geopolymers, this –OH stretching and bending are very low because of removal of water during post heat-treatment. For the ashes there are very small bands present around 1040–1080 cm^{-1} which is due to small level of Si–O–Si stretching vibrations. On the other hand these stretching vibrations are to a greater level present in both geopolymers. For both geopolymers, these Si–O–T (T: Si or Al) asymmetric stretching vibrations appear to be around 1000 cm^{-1} [22]. A band corresponding to Si–O–Al vibrations is present at 771 cm^{-1} in both geopolymers. A band around 1440 cm^{-1} is due to the presence of sodium carbonate. Shoulder between 810 and 1000 cm^{-1} is due to the presence of quartz, which is higher in

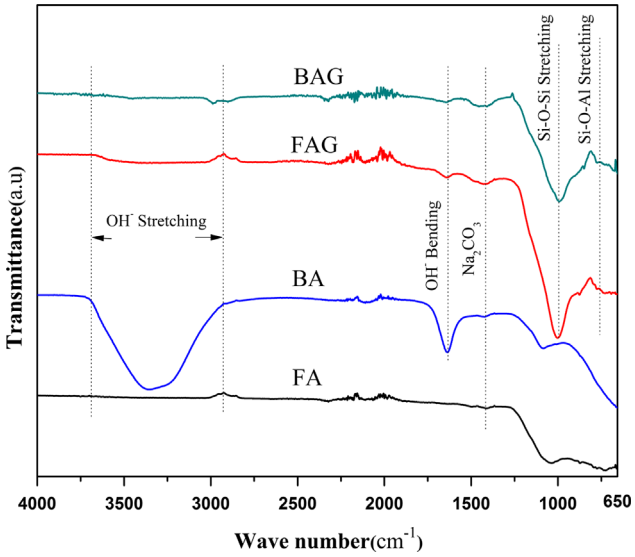

Fig. 5. FTIR of ashes and geopolymers.

Table 3
Inverted peak areas and peak heights' ratios of geopolymers at Si–O–Si stretching vibrations from IR spectra.

Sample ID	Wave number of Si–O–Si (cm^{-1})	Ratio of peak heights	Ratio of peak areas
FA	1035	1	1
FAG	1001	4.57	5.85
BA	1080	1	1
BAG	990	2.42	4.28

geopolymers compared to ashes, due to use of sodium silicate in geopolymer processing [23–25]. The degree of geopolymerization can be quantitatively indicated in terms of height ratios and area ratios of the Si–O–Si stretching peaks' present in the FTIR spectra of geopolymers to their corresponding ashes peaks. Calculated ratios are given in the Table 3. The ratios of peak heights and areas to their respective ashes are significantly higher, indicating the higher degree of geopolymerization in the samples. The geopolymerization level is lower in BAG compared to FAG, but still the polymerization level is higher than previous achieved results till date for BAG [26].

3.6. Morphological characterization by SEM

SEM micrographs were evaluated to investigate microstructure of the ashes and their geopolymers as shown in Fig. 6. Fly ash micrograph (Fig. 6a) shows numerous tiny spheres known as cenospheres, perfectly round smooth and intact. These spheres due to their higher surface area to volume ratio are more prone to move with air blast hence called fly ashes. On the other hand bottom ash particles are much larger, irregular and porous with many tiny pores visible in the microstructure (Fig. 6b). These are those tiny pores which contain absorbed water where water is not only adhered to surface but also absorbed because of its comparative porous nature. This water was detected by DTA, TGA and FTIR analysis. Since excess water might be detrimental to the geopolymers properties, care should be taken while using bottom ashes. They should either be dried prior to use or less amount of water should be used in the slurry. SEM image of FAG (Fig. 6c) reveals a relatively smooth structure compared to fly ash. This is because of full or partial dissolution of the spherical particles and regeneration of new microstructure during geopolymerization. But still many fine round particles, not attacked or partially attacked by the activating sodium hydroxide solution can be seen in the micrograph. Microstructure of BAG (Fig. 6d) shows much smooth and uniform surface as compared to FAG, because the whole mass was majorly composed of irregular particles and the reaction after activation produces a much more uniform structure. Besides uniform structure, small cracks are also visible in the microstructure of BAG which could be due to the shrinkage after loss of water during drying.

3.7. Density, porosity and thermal conductivity analysis

The bulk and the apparent densities were evaluated to investigate the porosity in both types of geopolymers. FAG samples are found to be more porous 37.5% than BAG with 33% porosity. Porosity values are considerably high, not only because of entrapped air during milling, but also due to post heat-treatment where water molecules create micropores during escape through the network. The bulk densities achieved for both geopolymers are lower than the previously reported values for the same composition [9]. Thermal conductivities of both types of geopolymers were measured using modified transient plan source techniques. FAG exhibits higher thermal insulation compared to BAG due to the presence of unreacted or partially reacted cenospheres and also because of higher porosity. Other factors like uniform microstructure (SEM analysis) and more crystallinity (XRD analysis) of BAG may influence its thermal conductivity properties. Bulk and apparent densities, percentage porosities and thermal conductivities of both types of geopolymers are given in the Table 4.

3.8. Compressive strength

The mechanical properties of geopolymers were evaluated through compression test, stress–strain curves are reported in Fig. 7. One of the interesting outcomes of this research is the high compressive strength (55.2 MPa) exhibited by the BAG, which is usually not comparable to FAG because of its low chemical reactivity. In our work the strength of BAG is near to FAG compressive strength (61.4 MPa) and is higher comparing to previously reported strength for BAG [11,12]. But still the strength for BAG is lesser than FAG perhaps because of inherent microcracks revealed in SEM analysis; produced during evaporation through uniform dense structure of BAG. Young's moduli are calculated by measuring the slopes of the uniform elastic regions on the stress–strain curves and the values are given in Table 4. Young's moduli for both BAG and

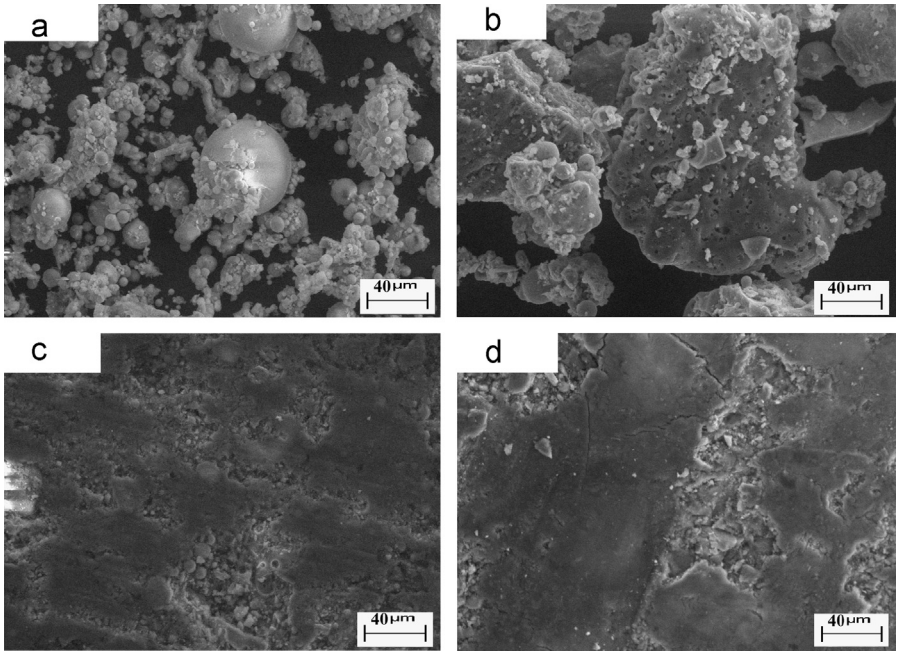

Fig. 6. SEM micrographs of ashes and respective geopolymers' microstructures.

Table 4
Physical and mechanical properties of geopolymers.

Sample ID	Apparent density (g/cm^3)	Bulk density (g/cm^3)	Porosity (%)	Thermal conductivity (W/mK)	Compressive strength (MPa)	Young's modulus (GPa)
FAG	2.45	1.454	37	0.58	61.4	2.9
BAG	2.48	1.65	33.5	0.848	55.2	2.8

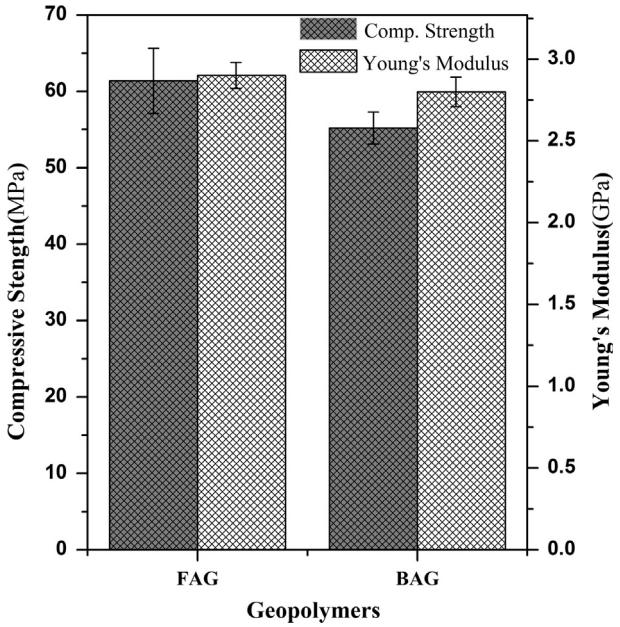

Fig. 7. Compressive strengths and Young's moduli of FAG and BAG.

FAG are in the range 2.8–2.9 GPa and these values are higher than the previously reported results [9,27]. The dehydroxylation during post heat-treatment creates micropores due to the escape of water molecules. This does not decrease the compressive strength instead the strength is increased due to formation of new Si–O–Si bonds.

4. Conclusion

Heat treatments and humidity content have significant effect over the mechanical and functional properties of geopolymers derived from fly and bottom ash. With the post heat-treatment, the Si–OH bonds transform to Si–O–T (T:Si or Al) type which give more stability, higher strength and rigidity. The higher Young's modulus is achieved using thermal curing due to higher degree of geopolymerization.

TGA, DTA and FTIR analyses show that similar kind of reactions and microstructures are formed during geopolymerization of fly ash and bottom ashes. FTIR analysis indicates the higher geopolymerization ability of fly ash but still the difference is not so significant. The same comparison we get in SEM analysis and compression test analysis. The FAG exhibit lower thermal conductivity because of the unreacted tiny spherical particular structure and also because of the larger porosity compared to BAG. The compressive strength of the BAG is 55.2 MPa while FAG exhibits 61.4 MPa which are close to each other. Having almost similar composition, fly ash and bottom ash can be equally valuable for the production of geopolymer mortar and concrete provided that process parameters are controlled in a proper way.

References

[1] M. Izquierdo, X. Querol, C. Phillipart, D. Antenucci, M. Towler, The role of open and closed curing conditions on the leaching properties of fly ash-slag-based geopolymers, Journal of Hazardous Materials 176 (2010) 623–628.

[2] R.N. Thakur, S. Ghosh, Effect of mix composition on compressive strength and microstructure of fly ash based geopolymer composites, ARPN Journal of Engineering and Applied Sciences 4 (2009) 68–74.
[3] M. Izquierdo, X. Querol, J. Davidovits, D. Antenucci, H. Nugteren, C. Fernández-Pereira, Coal fly ash-slag-based geopolymers: Microstructure and metal leaching, Journal of Hazardous Materials 166 (2009) 561–566.
[4] T. Bakharev, Thermal behaviour of geopolymers prepared using class F fly ash and elevated temperature curing, Cement and Concrete Research 36 (2006) 1134–1147.
[5] J. Somaratna, D. Ravikumar, N. Neithalath, Response of alkali activated fly ash mortars to microwave curing, Cement and Concrete Research 40 (2010) 1688–1696.
[6] S. Jumrat, B. Chatveera, P. Rattanadecho, Dielectric properties and temperature profile of fly ash-based geopolymer mortar, International Communications in Heat and Mass Transfer 38 (2011) 242–248.
[7] J. Temuujin, R.P. Williams, A. van Riessen, Effect of mechanical activation of fly ash on the properties of geopolymer cured at ambient temperature, Journal of Materials Processing Technology 209 (2009) 5276–5280.
[8] M.I.A. Aleem, P.D. Arumairaj, Geopolymer concrete – a review, International Journal of Engineering Science and Emerging Technologies 1 (2012) 118–122.
[9] J. Temuujin, A. van Riessen, K.J.D. MacKenzie, Preparation and characterisation of fly ash based geopolymer mortars, Construction and Building Materials 24 (2010) 1906–1910.
[10] P.K. Sarker, Analysis of geopolymer concrete columns, Materials and Structures 42 (2009) 715–724.
[11] P. Chindaprasirt, C. Jaturapitakkul, W. Chalee, U. Rattanasak, Comparative study on the characteristics of fly ash and bottom ash geopolymers, Waste Management 29 (2009) 539–543.
[12] H. Xu, Q. Li, L. Shen, W. Wang, J. Zhai, Synthesis of thermostable geopolymer from circulating fluidized bed combustion (CFBC) bottom ashes, Journal of Hazardous Materials 175 (2010) 198–204.
[13] A. Sathonsaowaphak, P. Chindaprasirt, K. Pimraksa, Workability and strength of lignite bottom ash geopolymer mortar, Journal of Hazardous Materials 168 (2009) 44–50.
[14] Y.J. Zhang, L.C. Liu, Y. Xu, Y.C. Wang, D.L. Xu, A new alkali-activated steel slag-based cementitious material for photocatalytic degradation of organic pollutant from waste water, Journal of Hazardous Materials 209– (210) (2012) 146–150.
[15] X. Guo, H. Shi, L. Chen, W.A. Dick, Alkali-activated complex binders from class C fly ash and Ca-containing admixtures, Journal of Hazardous Materials 173 (2010) 480–486.
[16] Q. Li, H. Xu, F. Li, P. Li, L. Shen, J. Zhai, Synthesis of geopolymer composites from blends of CFBC fly and bottom ashes, Fuel 97 (2012) 366–372.
[17] A. Medina, P. Gameroa, X. Querol, N. Moreno, B. De Leóna, M. Almanza, G. Vargasa, M. Izquierdo, O. Font, Fly ash from a Mexican mineral coal I: mineralogical and chemical characterization, Journal of Hazardous Materials 181 (2010) 82–90.
[18] B. Lothenbach, L. Pelletier-Chaignat, F. Winnefeld, Stability in the system $CaO–Al_2O_3–H_2O$, Cement and Concrete Research 42 (2012) 1621–1634.
[19] N. Billong, U.C. Melo, D. Njopwouo, F. Louvet, J.P. Bonnet, Effect of mixture constituents on properties of slaked lime–metakaolin–sand mortars containing sodium hydroxide, Cement and Concrete Composites 31 (2009) 658–662.
[20] V. Zivica, M.T. Palou, L. Bagel, M. Krizma, Low-porosity tricalcium aluminate hardened paste, Construction and Building Materials 38 (2013) 1191–1198.
[21] F. Skvára, L. Kopecky, V. Smilauer, Z. Bittnar, Material and structural characterization of alkali activated low-calcium brown coal fly ash, Journal of Hazardous Materials 168 (2009) 711–720.
[22] Y. Huang, M. Han, The influence of α-Al_2O_3 addition on microstructure, mechanical and formaldehyde adsorption properties of fly ash-based geopolymer products, Journal of Hazardous Materials 193 (2011) 90–94.
[23] E. Álvarez-Ayuso, X. Querol, F. Plana, A. Alastuey, N. Moreno, M. Izquierdo, O. Font, T. Moreno, S. Diez, E. Vazquez, M. Barra, Environmental, physical and structural characterisation of geopolymer matrixes synthesised from coal (CO–)combustion fly ashes, Journal of Hazardous Materials 154 (2008) 175–183.
[24] V.F.F. Barbosa, K.J.D. MacKenzie, C. Thaumaturgo, Synthesis and characterisation of materials based on inorganic polymers of alumina and silica: sodium polysialate polymers, International Journal of Inorganic Materials 2 (2000) 309–317.
[25] J.G.S. van Jaarsveld, J.S.J. van Deventer, G.C. Lukey, A comparative study of kaolinite versus metakaolinite in flyash based geopolymers containing immobilized metals, Chemical Engineering Communications 191 (2004) 531–549.
[26] U. Rattanasak, P. Chindaprasirt, Influence of NaOH solution on the synthesis of fly ash geopolymer, Minerals Engineering 22 (2009) 1073–1078.
[27] M. Komljenovic, Z. Bascarevic, V. Bradic, Mechanical and microstructural properties of alkali-activated fly ash geopolymers, Journal of Hazardous Materials 181 (2010) 35–42.